JOC The Journal of Organic Chemistry

Article

pubs.acs.org/joc

Increasing the Stability of DNA:RNA Duplexes by Introducing Stacking Phenyl-Substituted Pyrazole, Furan, and Triazole Moieties in the Major Groove

Mick Hornum, Pawan Kumar, Patricia Podsiadly, and Poul Nielsen*

Nucleic Acid Center, Department of Physics, Chemistry & Pharmacy, University of Southern Denmark, Campusvej 55, DK-5230 Odense, Denmark

Supporting Information

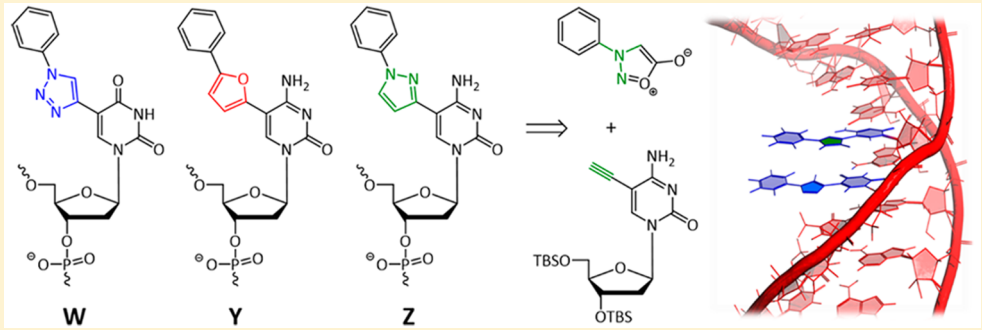

ABSTRACT: Consecutive incorporations of our previously published thymidine analogue, 5-(1-phenyl-1*H*-1,2,3-triazol-4-yl)-2′-deoxyuridine monomer **W** in oligonucleotides, has demonstrated significant duplex-stabilizing properties due to its efficient staking properties in the major groove of DNA:RNA duplexes. The corresponding 2′-deoxycytidine analogue is not as well-accommodated in duplexes, however, due to its clear preference for the ring-flipped coplanar conformation. In our present work, we have used *ab initio* calculations to design two new building blocks, 5-(5-phenylfuran-2-yl)-2′-deoxycytidine monomer **Y** and 5-(1-phenyl-1*H*-pyrazol-3-yl)-2′-deoxycytidine monomer **Z**, that emulate the conformation of **W**. These monomers were synthesized by Suzuki−Miyaura couplings, and the pyrazole moiety was obtained in a cycloaddition from *N*-phenylsydnone. We show that the novel analogues **Y** and **Z** engage in efficient stacking either with themselves or with **W** due to a better overlap of the aromatic moieties. Importantly, we demonstrate that this translates into very thermally stable DNA:RNA duplexes, thus making **Y** and especially **Z** good candidates for improving the binding affinities of oligonucleotide-based therapeutics. Since we now have both efficiently stacking T and C analogues in hand, any purine rich stretch can be effectively targeted using these simple analogues. Notably, we show that the introduction of the aromatic rings in the major groove does not significantly change the helical geometry.

INTRODUCTION

The high plasticity of oligonucleotides in combination with the high specificity of Watson−Crick hybridization have made oligonucleotides attractive agents for diagnostic[1] and therapeutic applications.[2,3] Indeed, siRNA[4] and antisense therapy[5] are promising alternatives to conventional chemotherapy of many genetic disorders (including Duchenne muscular dystrophy,[6] amyotrophic lateral sclerosis,[7] etc.), cancers,[8,9] viral infections,[10] and other diseases for which the target mRNA can be identified. However, for such oligonucleotides to become efficient therapeutic agents, they need to be chemically modified to optimize potency, biostability, absorption, and biodistribution.[11,12] A number of nucleic acid analogues such as LNA[13,14] have already provided oligonucleotides with significantly increased hybridization affinity toward RNA; some of these analogues are now widely used in many molecular biological technologies,[15] and some are entering clinics.[16] Although the hybridization characteristics are generally conserved, or even improved, by the use of such analogues, they often lead to structural and functional perturbation of the duplexes arising from their non-natural sugar−phosphate backbone. For many applications, however, it is important to maintain the native secondary structure of the duplex in order to preserve the biological activity. Less perturbing alternatives include modifications confined to the major groove faces of the nucleobases, such as the 5-position of pyrimidines or the 7-position of purines. In this way, the modified portion is placed discretely in the major grooves of duplexes, thereby minimizing the structural impacts on the duplex geometry as well as the Watson−Crick base pairs.

It is well-known that favorable stacking of the heterocyclic bases contributes most of the favorable enthalpy of duplex formation for nucleic acid duplexes.[17,18] Some efforts have been

Received: July 9, 2015
Published: September 3, 2015

DOI: 10.1021/acs.joc.5b01577
J. Org. Chem. 2015, 80, 9592−9602

made to enhance $\pi-\pi$ stacking in nucleic acids duplexes in order to increase the thermal stabilities of the duplexes, including the use of synthetic nucleobases with larger ring systems,[19] such as the tricyclic phenoxazine and phenothiazine nucleobase analogues.[20] More simple modifications have been to increase the aromatic systems by connecting small (hetero)aromatic moieties to the 5-position of pyrimidines.[21,22] Along these lines, we have previously shown that 1,2,3-triazoles,[23] and in particular 1-phenyl-1*H*-1,2,3-triazol-4-yl moieties[23−28] (monomers **W** and **X**; Figure 1), in the 5-position of 2′-deoxyuridine and 2′-deoxycytidine engage in efficient $\pi-\pi$ stacking in the major groove, which in turn translates into high-affinity RNA recognition whenever two or more of these building blocks are placed adjacently. In addition, oligonucleotides bearing these building blocks show intact base pairing fidelity and high stability toward nucleolytic degradation,[25] making them excellent candidates in siRNA or antisense designs.

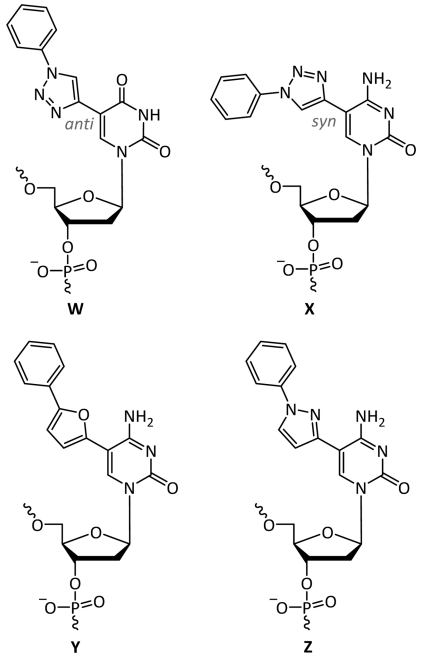

Figure 1. Structures of monomers **W**, **X**, **Y**, and **Z**.

Interestingly, we have shown that the DNA:RNA duplex formation is significantly compromised if the linking triazole group is either absent or even just inversed.[27] Even more delicately, we have shown that even the precise torsion of the phenyltriazole moiety is crucial for optimal duplex stability, since the subtle different orientations of the phenyltriazole moieties in monomers **W** and **X** give rise to significant differences in the thermal stability of the duplex. The preferred *anti* torsion of the 5-substituent of monomer **W** places the phenyl group toward the core of the duplex, whereas the preferred *syn* torsion of monomer **X** (Figure 1) points the phenyl group slightly away from the helical axis.[25] The *anti* torsion appears to be much better accommodated by DNA:RNA duplexes, as evidenced by comparing the changes in melting temperatures following single (**W**, ΔT_m = +1.8 °C; **X**, ΔT_m = −2.5 °C) and multiple (**WWWW**, ΔT_m = +13.3 °C; **XXXX**, ΔT_m = +4.9 °C) incorporations of **W** and **X** centrally in a 16-mer DNA:RNA duplex.[25]

In the present study, we have searched for alternative C building blocks that are structurally and conformationally similar to building block **W** in order to track down a simple C building block with potentially optimized stacking interactions in the major groove. After conformational analyses, we have designed two new C building blocks: 5-(2-phenylfuran-5-yl)-2′-deoxycytidine monomer **Y** and 5-(1-phenyl-1*H*-pyrazol-3-yl)-2′-deoxycytidine monomer **Z** (Figure 1). First of all, we demonstrate that these building blocks are well-accommodated in DNA:RNA duplexes because of their *anti* positioning of the phenyl substituent. This conformation places the phenyl group into the hollow core of the major groove resembling monomer **W**. Interestingly, we show that when **W** and **Y** and in particular **W** and **Z** are placed adjacently in a 16-mer DNA:RNA duplex, this geometrically optimized aromatic overlap translates into significantly increased thermal stabilities of the duplexes relative to the native ones without compromising the helical geometry.

RESULTS

Conformational Analyses. In continuation of our previous conformational studies on phenyltriazoles,[23,25,27] we decided to use *ab initio* calculations to quantify the conformational behaviors of potential five-membered aromatic heterocycles directly attached to the 5-position of cytosine, in order to find optimal candidates for a new C building block based on the torsional profiles. Specifically, eight heterocycles were selected and scanned for their tendency to form a torsional angle (θ) of 180° (*anti*) defined by the substituted face of the 5-heterocycle and the C5,C6 face of cytosine. The choice of heterocycles for the study was based on their likely capability of adopting an *anti* conformation stabilized by an intermolecular O/N (heterocycle)−HN (cytosine) hydrogen bond. All calculations were performed at MP2/6-31G** in vacuum using simplified derivatives of each compound.

In the case of all eight selected dimethylated heterocycle-cytosine models, a clear preference for the *anti* conformation of the C5−heterocycle bond was observed (see Figure S1 in Supporting Information). Of the eight structures, 1-methyl-5-(1-methyl-1*H*-pyrazol-3-yl)cytosine (representing monomer **Z**; blue curve in Figure 2) showed a pronounced clear preference for *anti* with a very deep global minimum at θ = 180° and with the highest global maximum at θ = 0° of all the modeled structures. The clear preference for the *anti* conformer suggests that monomer **Z** is inclined to be geometrically similar to **W** (black dashed line in Figure 2), which is essential for an efficient aromatic overlap of the two residues. Similar energy profiles, with a deep global minimum at θ = 180° and a global maximum at θ = 0°, were obtained for three oxazole or thiazole cytosine models (Figure S1, B-type profile).

Three other of the modeled structures, e.g., 1-methyl-5-(5-methylfuran-2-yl)cytosine (representing monomer **Y**; red curve in Figure 2), showed energy profiles with very wide minima at θ = 180° (Figure S1, A-type profile). In these cases, the global minima are in fact shifted slightly away from coplanarity by about ±30°; however, the low barrier separating the minima (ΔE = 1−2 kJ/mol) means that they can essentially be treated as a flat energy surface from 135° to 225°, indicating that they have a high degree of rotational freedom in their *anti* conformations. Although this less favorable energy profile does not directly advocate efficient stacking, it nevertheless suggests that the aromatic 5-substituents of these building block may be able to adapt to their surrounding aromatic moieties, and in this way potentially improve the π stacking interactions. Accordingly, we decided to synthesize and incorporate both monomers **Y** and **Z**,

DOI: 10.1021/acs.joc.5b01577
J. Org. Chem. 2015, 80, 9592−9602

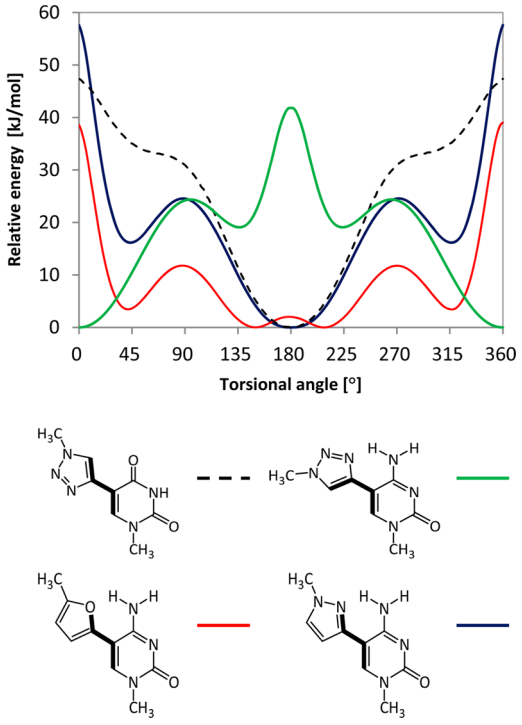

Figure 2. Energy scans of the torsion θ making up the single bond between the two heterocycles of model compounds of **W**, **X**, **Y**, and **Z** calculated using the MP2/6-31G** level. The illustrated structures are drawn in their lowest-energy conformations.

the most appealing representatives of each energy profile types, in duplexes to evaluate their stacking promise *in vitro*.

Synthesis. Oligonucleotides containing monomers **W**, **Y**, and **Z** were synthesized on solid-phase using the natural phosphoramidites along with the customized phosphoramidites **6** and **14** (Scheme 1) as well as the phosphoramidite of monomer **W**. The phosphoramidite of **W** was synthesized from 5′-*O*-DMT-protected 5-ethynyl-2′-deoxyuridine in a CuAAC reaction[29,30] with azidobenzene, followed by a 3′-*O*-phosphitylation, using an improved protocol of our previous reported procedure[23] (see Supporting Information and Experimental Section).

Phosphoramidite **6** was conveniently synthesized by a Suzuki–Miyaura cross-coupling approach starting from the totally deprotected 5-iodo-2′-deoxycytidine (**1**) and commercial 5-phenylfuran-2-boronic acid pinacol ester (**2**). This Pd-catalyzed reaction was initially carried out in polar aprotic solvents; however, in general, poor conversion of the starting materials was observed under all reaction conditions, and chromatographic separation from the residual starting material was difficult. Realizing that the reaction progress was slightly improved in water–organic cosolvent mixtures, we eventually investigated the reactivity in pure water akin to Len and co-workers.[31] Using 10 mol % loading of the water-insoluble catalyst, $Pd(PPh_3)_4$, and 2 equiv of NaOH, we remarkably observed full conversion of the starting material **1** after just 60 min at 70 °C under microwave irradiation. A solid precipitated from the water upon cooling of the reaction mixture, which, when washed with a small amount of CH_2Cl_2 to remove the catalyst, was found to be pure 5-(5-phenylfuran-2-yl)-2′-deoxycytidine (**3**) in 75% yield. The reaction has been found to be very robust, consistent, and scalable, and the fact that the reaction proceeds in pure water solvent and without extractive

Scheme 1[a]

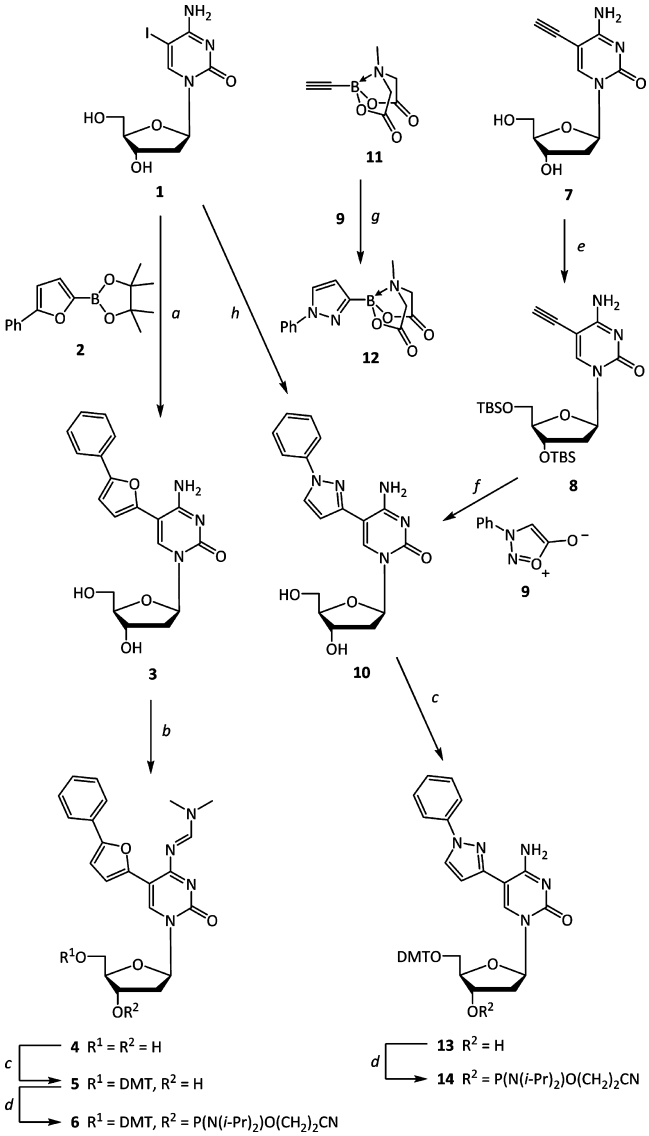

[a]Reagents and conditions: (a) **2**, $Pd(PPh_3)_4$, NaOH, H_2O, 70 °C, MW, 1 h, 75%; (b) *N*,*N*-dimethylformamide dimethylacetal, DMF, 55 °C, 2 h, 98%; (c) DMTCl, pyridine, rt, 16 h, 66% **5**, 38% **13**; (d) $P(N(i\text{-}Pr)_2)O(CH_2)_2CN$, diisopropylammonium tetrazolide, CH_2Cl_2, rt, 18 h, 70% **6**, 64% **14**; (e) TBSCl, imidazole, DMF, rt, 16 h, 95%; (f) **9**, 1,2-dichlorobenzene, 180 °C, MW, 4 h; then TBAF, THF, rt, 1 h, 29% (two steps); (g) **9**, anisole, 165 °C, 36 h, 53%; (h) **12**, $Pd(PPh_3)_4$, K_3PO_4, DMF, H_2O, 60 °C, 48 h, 80%. DMT = 4,4′-dimethoxytrityl.

or chromatographic workup makes this reaction a remarkably convenient and green way to install a phenylfuran moiety to the 5-position of 2′-deoxycytidine. Nucleoside **3** was subsequently protected with an amidine protecting group[32] using *N*,*N*-dimethylformamide dimethyl acetal in DMF in 98% yield, followed by a 5′-*O*-selective tritylation using DMTCl in pyridine to furnish the protected nucleoside **5** in 66% yield. Finally, conversion into the corresponding 3′-*O*-phosphoramidite (**6**) by treatment with 2-cyanoethyl *N*,*N*,*N*′,*N*′-tetraisopropylphosphorodiamidite (PN2) and diisopropylammonium tetrazolide in CH_2Cl_2 proceeded in 70% yield.

For the synthesis of nucleoside **10** we investigated the use of a thermal [2 + 3] sydnone–alkyne cycloaddition[33] between 5-ethynyl-2′-deoxycytidine[34] (**7**) and *N*-phenylsydnone (**9**),[35]

DOI: 10.1021/acs.joc.5b01577
J. Org. Chem. 2015, 80, 9592–9602

which is a stable synthetic equivalent of the corresponding azomethine imine, in order to construct the pyrazole ring at the nucleoside level, akin to the alkyne−azide click reactions used for the synthesis of the triazoles in **W** and **X**.[23,25] Nucleoside **7** was protected to enhance the solubility in organic solvents and to avoid nucleophilic opening of the mesoionic ring structure under the high temperatures. In a series of attempts using various temperatures (140−240 °C) and nonpolar solvents (xylenes, toluene, 1,2-dichlorobenzene, anisole), it was found that the cycloaddition proceeded optimally under microwave-mediated heating to 180 °C in 1,2-dichlorobenzene and by the use of transient *tert*-butyldimethylsilyl protecting groups for the 3′ and 5′ alcohols (compound **8**), which were found to be superior to acetyl protecting groups. Although we did not manage to drive the cycloaddition to completion, 5-(1-phenyl-1*H*-pyrazol-3-yl)-2′-deoxycytidine (**10**) was obtained in 29% isolated yield following the subsequent desilylation. Also, 15% of the corresponding 1,4-substituted pyrazole isomer was obtained, but the two regioisomers could be separated by silica gel chromatography. The two regioisomers were easily resolved on the basis of the dissimilar ^{1}H NMR coupling constants for the two protons in their respective pyrazole rings: $^3J_{HH}$ = 2.5 Hz for the 1,3-substituted pyrazole (nucleoside **10**) and $^4J_{HH}$ ∼ 0−0.1 Hz for the 1,4-substituted pyrazole. Despite the recent development of Cu-promoted sydnone−alkyne cycloadditions,[36,37] no improvements in terms of reactivity or regioselectivity were observed by the use of stoichiometric amounts of $Cu(OTf)_2$ or a few other Lewis acids.

To the best of our knowledge, we demonstrate here for the first time the successful use of sydnone-alkyne cycloadditions for the introduction of pyrazole rings into a highly functionalized molecule. Although the isolated yield for the particular reaction is rather low, this thermal cycloaddition strategy nevertheless provides a feasible entry for pyrazole-functionalized nucleosides from two simple starting materials (most of which could also be recovered and recycled). In order to validate its potential on other nucleoside substrates, we also attempted the cycloaddition of *N*-phenylsydnone (**9**) with 5-ethynyl-2′-deoxyuridine (**15**) to successfully form 5-(1-phenyl-1*H*-pyrazol-3-yl)-2′-deoxyuridine (**17**) in 41% yield over three steps (Scheme 2). Also, small amounts of the corresponding 1,4-substituted pyrazol isomer were obtained.

In order to optimize yields for the synthesis of nucleoside **10**, we also investigated a Suzuki−Miyaura approach similar to the synthesis of nucleoside **3** (Scheme 1). Due to the lack of a commercial pyrazole equivalent of boronic acid pinacol ester **2**, we instead focused on the corresponding pyrazole MIDA boronate **12**, the preparation and reactivity of which are known in the literature.[38] Accordingly, the sydnone−alkyne cycloaddition between commercial ethynylboronic acid MIDA ester (**11**) and *N*-phenylsydnone (**9**) in anisole furnished compound **12**, which was used for the subsequent Suzuki−Miyaura reaction (Scheme 1). The MIDA boronate was found to be quickly hydrolyzed and protodeboronated in aqueous NaOH solutions, which severely hampered the reaction efficiency. However, with the use of a K_3PO_4-mediated[39] *in situ* slow release of the unstable boronic acid, nucleoside **10** was obtained in 80% yield from 5-iodo-2′-deoxycytidine (**1**) after 48 h at 60 °C in a mixture of DMF and H_2O (7:1) with 20 mol % of $Pd(PPh_3)_4$.

Nucleoside **10** was protected with a 5′-*O*-DMT group using DMTCl in pyridine to obtain nucleoside **13** in 38% yield with recovery of 52% unreacted nucleoside **10**. The use of alternative systems (Et_3N, imidazole/CH_2Cl_2, 2,6-lutidine/DMSO, DMAP/pyridine or $AgNO_3$/pyridine) or higher temperatures did not increase the isolated yield of nucleoside **13**, in most cases due to significant formation of the doubly or even triply protected nucleoside products. Finally, nucleoside **13** was phosphitylated at the 3′-position by PN2 to furnish the base-unprotected phosphoramidite **14** in 70% yield. Puzzlingly, all attempts to install acyl, carbamate, or amidine protecting groups onto the nucleobase of **10** were unsuccessful, since the protecting groups were found to be too labile, seemingly due to their close proximity to the nucleophilic *N*2 (pyrazole) position allowing for 6-*endo-trig*- or 6-*exo-trig*-type cyclizations, followed by hydrolysis. This issue was not observed in the case of nucleoside **3**. We eventually decided to attempt oligonucleotide synthesis with the base-unprotected phosphoramidite **14**, inspired by the published protocols for oligonucleotide synthesis using phosphoramidites with unprotected bases.[40−42]

All phosphoramidites were successfully activated with 1*H*-tetrazole in MeCN for the solid-phase oligonucleotide syntheses. As expected, a significant amount of the *N*-phosphitylated oligonucleotide products were formed whenever phosphoramidite **14** was used. Although these defective oligonucleotides could be removed from the desired oligonucleotide later on by reversed-phase HPLC purification, we found to our delight that replacing 1*H*-tetrazole with 1-hydroxybenzotriazole (HOBt) in MeCN-DMF (15:1, v/v) (inspired by Sekine and co-workers[42]) provided 5′-*O*-specific condensation of the upstream phosphoramidites without compromising coupling yields. Accordingly, all three customized phosphoramidites were efficiently incorporated into the 16-mer oligonucleotides listed in Table 1 in excellent yields (>92%) using extended coupling times (20 min). The structures and the purities of the synthesized oligonucleotides were verified by MALDI-TOF MS analysis and anion-exchange HPLC (see Supporting Information).

Thermal Denaturation Studies. The synthesized oligonucleotides listed in Table 1 were mixed in medium salt buffer [Na_2HPO_4 (2.5 mM), NaH_2PO_4 (5 mM), NaCl (100 mM), EDTA (0.1 mM), pH 7] with their complementary single-stranded RNA and DNA sequences using 1.5 μM concentrations of each strand. Melting temperatures (T_m's) of the resulting duplexes (Table 1, entries 2−18 for DNA:RNA, and Table S1, entries 2−18 for DNA:DNA) were derived from the UV melting curves at 260 nm and compared with the native duplex (Table 1/Table S1, entry 1).

As shown in Table 1, a single incorporation of C building blocks **Y** and **Z** decreases the stability of the DNA:RNA duplexes by −1.9 and −0.5 °C, respectively (entries 4 + 5),

Scheme 2[a]

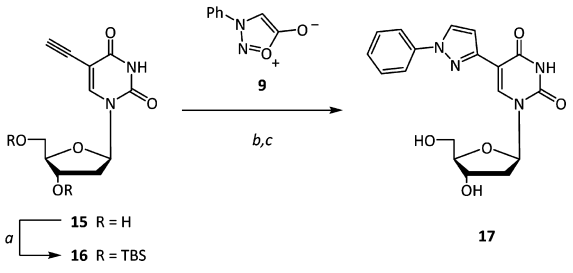

[a](a) TBSCl, imidazole, DMF, rt, 4 h, quantitative; (b) **9**, 1,2-dichlorobenzene, 200 °C, MW, 5 h; (c) TBAF, THF, rt, 1 h, 41% (two steps).

DOI: 10.1021/acs.joc.5b01577
J. Org. Chem. 2015, 80, 9592−9602

Table 1. Melting Temperatures of the Synthesized DNA:RNA Duplexes[a]

entry	ON sequences	T_m (ΔT_m/mod) [°C]
1	5′-d(TTTTCTTTTCCCCCCT)	62.7[b] or 60.0
2	5′-d(TTTTCTTT**W**CCCCCCT)	64.5[b] (+1.8)
3	5′-d(TTTTCTTTT**X**CCCCCT)	60.2[b] (−2.5)
4	5′-d(TTTTCTTTT**Y**CCCCCT)	58.1 (−1.9)
5	5′-d(TTTTCTTTT**Z**CCCCCT)	59.5 (−0.5)
6	5′-d(TTTTC**WWWW**CCCCCCT)	76.0[b] (+3.3)
7	5′-d(TTTTCTTTT**XXXX**CCT)	67.6[b] (+1.2)
8	5′-d(TTTTCTTTT**YYYY**CCT)	66.7 (+1.7)
9	5′-d(TTTTCTTTT**ZZZZ**CCT)	72.3 (+3.1)
10	5′-d(TTT**WX**TTTTCCCCCCT)	68.7[b] (+3.0)
11	5′-d(TTT**WY**TTTTCCCCCCT)	63.8 (+1.9)
12	5′-d(TTT**WZ**TTTTCCCCCCT)	64.9 (+2.5)
13	5′-d(TTTT**XW**TTTCCCCCCT)	66.7[b] (+2.0)
14	5′-d(TTTT**YW**TTTCCCCCCT)	63.1 (+1.6)
15	5′-d(TTTT**ZW**TTTCCCCCCT)	65.4 (+2.7)
16	5′-d(TTT**WXW**TTTCCCCCCT)	70.9[b] (+2.7)
17	5′-d(TTT**WYW**TTTCCCCCCT)	67.6 (+2.5)
18	5′-d(TTT**WZW**TTTCCCCCCT)	70.2 (+3.4)

[a]Melting temperatures (T_m's) for DNA:RNA duplexes were obtained from the maxima of the first derivatives of the absorbance (260 nm) vs temperature curves. The samples contained 1.5 μM of each oligonucleotide and 1.5 μM of complementary RNA 5′-r-(GGGGGGAAAAGAAAA) in a phosphate buffered saline solution (2.5 mM Na_2HPO_4, 5.0 mM NaH_2PO_4, 100 mM NaCl, 0.1 mM EDTA, pH 7.0). Values in brackets show changes in the T_m values per modification compared to the unmodified duplex. [b]This value is taken from ref 25 and is included in the table for comparison.

which are both less destabilizing than monomer **X** (ΔT_m = −2.5 °C, entry 3), but more destabilizing than a single incorporation of T building block **W** (ΔT_m = +1.8 °C, entry 2) in this sequence context. In turn, four consecutive incorporations of **Y** and **Z** increase the melting temperature of the duplexes by +1.7 and +3.1 °C per modification (entries 8 + 9), which shows that the thermal penalty of the incorporation appears to be more than compensated by the improved π−π stacking of the aromatic moieties. Importantly, the thermal stability of the duplex featuring four **Z** residues practically reaches that of the duplex featuring four **W** residues (ΔT_m = +3.3 °C/mod, entry 6), which is remarkable considering the significant greater change in the ΔT_m upon going from 1 to 4 modifications [**W**, $\Delta\Delta T_m$/mod = +1.5 °C (entry 2 vs 6); **Z**, $\Delta\Delta T_m$/mod = +3.6 °C (entry 5 vs 9)].

The three consecutive mixed stacking moieties **WYW** and **WZW** increase the T_m's by +2.5 and +3.4 °C per modification (entries 17 + 18), respectively, relative to the unmodified duplexes. This should be compared to the increase of +2.7 °C per modification that was observed for the duplex featuring **WXW** (entry 16). Thus, it appears that the expected better aromatic overlap observed between the **W** and **Z** residues indeed translates into a more thermally stable duplex in the case of the **WZW** motif. On the other hand, the **WYW** motif is slightly less stabilizing than **WXW**, which suggests that the rotationally less restricted phenylfuran moiety causes less efficient stacking of the aromatic 5-substituents. The same general tendency in the thermal stability is seen for the DNA:RNA duplexes featuring the 5′-**XW**, 5′-**YW**, and 5′-**ZW** motifs (entries 13−15). In the case of the 5′-**WX**, **WY**, and **WZ** motifs (entries 10−12), however, the 5′-**WX** motif is slightly better accommodated than the 5′-**WZ** motif, possibly reflecting the different stacking proportions of the aromatic moieties in the right-handed helix.

The T_m values of the DNA:DNA homoduplexes (Table S1) featuring **Y** and **Z** show the overall same trend as their corresponding DNA:RNA hybrid duplexes; however, the effect of the stacking aromatic moieties appears less significant.

CD Spectroscopy. All synthesized DNA:RNA duplexes were studied by CD spectroscopy in order to examine how the modifications affect the overall conformation and secondary structure of the duplexes. The CD spectra were recorded at 20 °C in medium salt buffer [Na_2HPO_4 (2.5 mM), NaH_2PO_4 (5 mM), NaCl (100 mM), EDTA (0.1 mM), pH 7] using 1.5 μM concentrations of each strand. The obtained CD spectra of the duplexes concerning **Y** are shown in Figure 3, and the spectra concerning **Z** are shown in Figure 4. CD spectra of duplexes featuring only **X** and **W** residues can be found in ref 25.

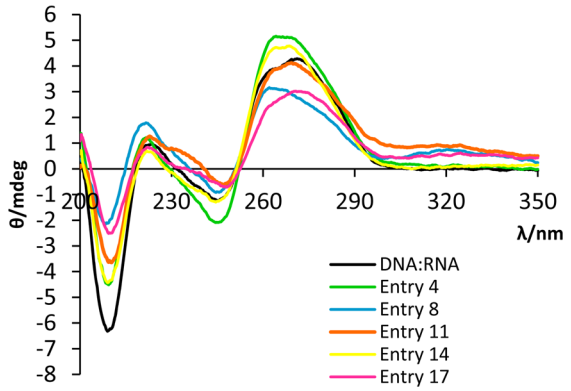

Figure 3. CD spectra of DNA:RNA duplexes featuring single (entry 4) and multiple (entry 8) incorporations of monomer **Y**, as well as duplexes containing consecutive **W** and **Y** building blocks (entry 11 + 14 + 17). The CD spectrum of the unmodified DNA:RNA duplex (entry 1) is shown in black. Entry numbers refer to Table 1.

As expected, the CD spectrum of the unmodified duplex (black curve) adopts bands that are characteristic of an A/B-type helix, including CD maxima near 270 nm (A-type) and 220 nm (B-type), CD minima near 245 nm (B-type) and 210 nm (A-type), and a clear crossover point (from positive to negative intensity) at 250 nm, in agreement with a typical DNA:RNA CD

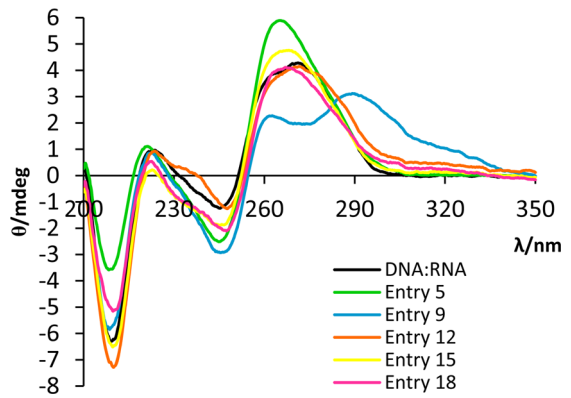

Figure 4. CD spectra of DNA:RNA duplexes featuring single (entry 5) and multiple (entry 9) incorporations of monomer **Z**, as well as duplexes containing consecutive **W** and **Z** building blocks (entry 12 + 15 + 18). The CD spectrum of the unmodified DNA:RNA duplex (entry 1) is shown in black. Entry numbers refer to Table 1.

DOI: 10.1021/acs.joc.5b01577
J. Org. Chem. 2015, 80, 9592−9602

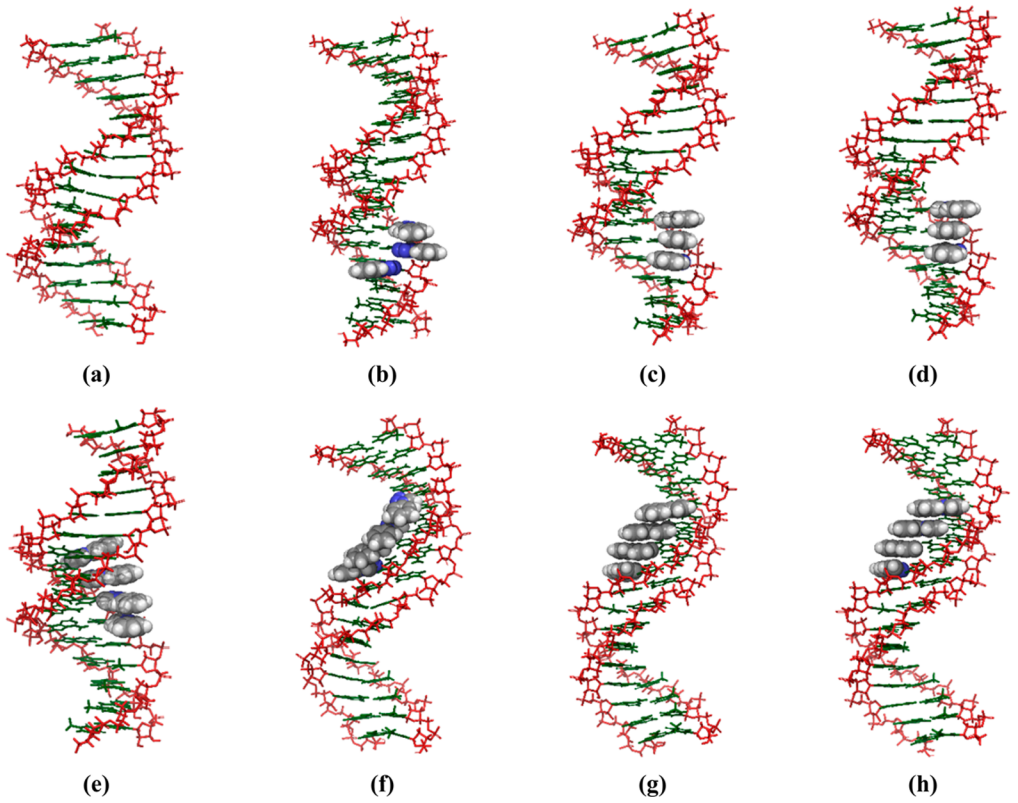

Figure 5. Global minimum structures obtained by 5 ns MD simulations of selected DNA:RNA duplexes from Table 1: (a) entry 1, (b) entry 16, (c) entry 17, (d) entry 18, (e) entry 6, (f) entry 7, (g) entry 8, (h) entry 9. The calculations were performed at 300 K using the all-atom AMBER* force field. The 5-substituents are shown with space-filling.

spectrum.[43] As shown in both figures, the CD spectra of the modified duplexes are strikingly similar to the CD spectrum of the unmodified duplex, suggesting that the geometry changes imposed by the modifications are indeed subtle. In fact, there appears to be no general shift toward either an A- or B-type helix in any of the duplexes. The most remarkable deviation from the standard A/B-type profile is observed in the duplex featuring four consecutive **Z** residues (Figure 4, entry 9), which contains a significant positive band at 290 nm and a shoulder at 260 nm. This new band appears to reflect local changes in the duplex conformation due to stacking phenylpyrazole moieties.

Molecular Dynamics Simulations. To gain more information about the geometries of the duplexes featuring three and four consecutive modifications (Table 1, entries 6−9 and 16−18), a series of 5 ns molecular dynamics simulations were performed. Using the all-atom AMBER* force field (MacroModel V10.4, release 2014-2) on the structures in GB/SA solvation, truthful global minimum structures of the modified DNA:RNA duplexes in solution were obtained, allowing us to visualize the degree of stacking of the 5-substituents in the duplex as well as suggesting how the modifications may influence the helical topology. The minimized structures from the MD simulations are shown in Figure 5. Top views are shown in Figure S2.

As expected, the modeled DNA:RNA duplexes are all found to be A/B-type helices with their 5-substitutents pointing into the major grooves. In agreement with the CD spectra, the modifications do not significantly alter the geometries of the duplexes, except for a slight narrowing of the minor grooves at the sites of the modifications. As previously shown by molecular modeling,[23,25] four consecutive incorporations of monomers **X** and especially **W** stack efficiently in the major groove (Figure 5e,f), and the present results show that also consecutive incorporations of monomer **Y** and **Z** are able to stack very efficiently (Figure 5g,h). As expected, the overall aromatic overlaps in the **WYW** (Figure 5c) and **WZW** (Figure 5d) motifs are much more efficient than the overlap in the **WXW** motif (Figure 5b), due to the *anti* conformation of the 5-substituents of the former two. However, in the case of the **WYW** motif, the **Y** residue appears to be wobbling throughout the simulation (as hinted by the *ab initio* calculations), and this may help explain why the thermal stability of the duplex featuring the **WYW** motif (Table 1, entry 17) is slightly reduced relative to that of the **WZW** motif (Table 1, entry 18).

DISCUSSION

In this study, we have applied molecular modeling, CD spectroscopy, and experimental melting temperatures to investigate how heteroaromatic moieties attached to the 5-position of pyrimidine nucleobases are accommodated in DNA:RNA duplexes. Specifically, we have introduced two new 5-substituted-2′-deoxycytidine monomers **Y** and **Z**, which in turn place phenylfuran and phenylpyrazole moieties in the major groove of the duplexes. These two monomers were selected after *ab initio* studies of a pool of eight model compounds due to their clear preferences for the *anti* torsion of their 5-substituents, but with different rotational degrees of freedom: the phenylfuran moiety of monomer **Y** is significantly more free than the phenylpyrazole monomer **Z**. These two new building blocks are synthesized in a few steps from commercially available starting materials. For the synthesis of monomer **Z**, we report the first use of a sydnone species reacting with a

DOI: 10.1021/acs.joc.5b01577
J. Org. Chem. 2015, 80, 9592−9602

nucleoside in a cycloaddition. This approach is strategically similar to the azide−alkyne cycloaddition we have previously used for the syntheses of monomers **W** and **X**.[23,25] Also remarkably, this study addresses the necessary but convenient use of the *N*-unprotected phosphoramidite **14** as a substrate for oligonucleotide synthesis. Successful 5′-*O*-selective condensation was achieved just by replacing the usual 1*H*-tetrazole activator with HOBt, requiring no changes in the settings of the synthesizer, and regular *N*-protected phosphoramidites were used for the unmodified nucleotides without loss in coupling yields.

From the hybridization studies, it is apparent that a single incorporation of either monomer **Y** and **Z** leads to a small decrease in the thermal stability of the duplex, possibly due to distortion of the hydration of the major groove. However, consecutive incorporations of either monomer **Y** and **Z** evoke stabilizing effects due to favorable stacking of the aromatic moieties, which more than compensates for the penalty of placing the hydrophobic 5-substituents in contact with water. The degree of stacking appears better in the case of monomer **Z** than in the case of **Y**, suggesting that the phenylfuran moiety of **Y** is too flexible for efficient $\pi-\pi$ stacking interactions. This also establishes a clear connection between the rotational profile and the efficiency of stacking. Importantly, the stabilizing effects of consecutive **Z** residues are noticeably superior to our previously published C analogue **X**, and the stability gain is comparable to our previously published T analogue **W**. The potential of monomer **Z** is particularly clear when it is placed next to monomer **W**, where an increased aromatic overlap between the two similar-oriented 5-substituents appears to be the explanation for a significantly increased T_m. In fact, the significant stabilizing effect triggered by the **WZW** motif (ΔT_m/mod = +3.4 °C), roughly similar to those of **WWWW** (ΔT_m/mod = +3.3 °C) or **ZZZZ** (ΔT_m/mod = +3.1 °C), signifies the favorable π stacking interactions between these two T and C analogues. Thus, monomer **Z** is well-suited as a complement to monomer **W** in, e.g., RNA-targeting oligonucleotides for obtaining high-affinity binding to complementary mixed purine sequences. Notably, the T_m values of the sequence-identical DNA:DNA duplexes are not nearly as stabilized by the stacking aromatic moieties, indicative of preferential recognition of RNA over DNA, possibly due to the more compressed character of the A-type duplex over the B-type.

As ascertained by CD spectroscopy and MD simulations, the incorporation of the **W**, **Y**, and **Z** residues into the duplexes does not significantly alter the geometries of the DNA:RNA duplexes relative to the native DNA:RNA duplex, which is opposed to many other known duplex stabilizing building blocks such as LNA.[44] Even so, the simple 5-modified pyrimidine building blocks presented herein can also easily be used in combination with other modifications such as phosphorothioates or LNA, e.g., in therapeutic oligonucleotides.

CONCLUSION

In this study, we have investigated the directional influence of phenyl-substituted heterocycles attached to the 5-position of pyrimidines in perfecting the stacking of the aromatic moieties in the major groove of DNA:RNA duplexes. Of the two new C building blocks **Y** and **Z** presented herein, monomer **Z** containing a phenylpyrazol moiety was found to engage in highly favorable $\pi-\pi$ stacking interactions in the major groove with itself and with an adjacent T building block **W**. Notably, no significant change in the duplex geometry was observed, as shown by CD spectroscopy and molecular modeling. The highly stabilizing effects observed for duplexes containing consecutive **W** and **Z** residues appear to be due to a large aromatic overlap of their 5-substituents. This makes the combination of the triazole-functionalized thymidine analogue **W** and the pyrazole-functionalized 2′-deoxycytidine analogue **Z** a simple tool in high-affinity RNA-targeting oligonucleotides. In principle, a long array of these stacking aromatic moieties can be used without compromising the duplex geometry.

EXPERIMENTAL SECTION

All reagents were used as supplied except CH_2Cl_2, which was distilled prior to use. Microwave irradiated reactions were conducted in sealed reaction vessels in a Biotage Initiator$^+$ instrument using external surface sensor probes. All reactions were monitored by TLC using silica gel (60 F_{254}) precoated plates. Column chromatography was performed using silica gel 60 (particle size 0.040−0.063 mm). For the purification of DMT-protected nucleosides, the silica gel was pretreated with pyridine/CH_2Cl_2 (1:100, v/v). After chromatography, appropriate fractions were combined and concentrated. All products were dried in high vacuum (<1 mm Hg) overnight to give products in high analytical purity. HRMS-ESI was recorded on a quadrupole time-of-flight instrument in positive ion mode with an accuracy of ±5 ppm. ^{1}H, ^{13}C, and ^{31}P NMR spectra were recorded at 400.12, 100.62, and 161.97 MHz, respectively. Chemical shifts are reported in ppm relative to tetramethylsilane ($\delta_{H,C}$ 0 ppm) or the deuterated solvents (DMSO δ_c 39.5 ppm, $CDCl_3$ δ_c 77.16 ppm). For ^{31}P NMR spectra, 85% H_3PO_4 was used as external standard. 2D spectra (HSQC, COSY, and HMBC) have been used in assigning ^{1}H and ^{13}C NMR signals.

5-(5-Phenylfuran-2-yl)-2′-deoxycytidine (3). 5-Iodo-2′-deoxycytidine (**1**, 300 mg, 0.85 mmol) was dissolved in an aqueous solution of NaOH (0.2 M, 4.25 mL, 0.85 mmol), and the solution was completely degassed with N_2. 5-Phenylfuran-2-ylboronic acid pinacol ester (**2**, 275 mg, 1.02 mmol) and $Pd(PPh_3)_4$ (98 mg, 85 μmol) were added, and the suspension was stirred under microwave irradiation for 60 min at 70 °C. The resulting yellow solution was cooled by N_2 flow for 15 min, and the resultant white precipitate was filtered off, washed with cold CH_2Cl_2 (5 × 5 mL) and cold water (2 × 5 mL), and dried under vacuum to obtain nucleoside **3** as a white solid (234 mg, 0.63 mmol). Yield: 75%. R_f 0.3 (6% MeOH in CH_2Cl_2). ^{1}H NMR (400 MHz, DMSO-d_6): δ 8.41 (s, 1H, H6), 7.76 (d, J = 7.5 Hz, 2H, H2 Ph), 7.73 (br, 1H, NH), 7.42 (t, J = 7.5 Hz, 2H, H3 Ph), 7.29 (t, J = 7.5 Hz, 1H, H4 Ph), 7.04 (d, J = 3.5 Hz, 1H, H4 furan), 6.75 (br, 1H, NH), 6.74 (d, J = 3.5 Hz, 1H, H3 furan), 6.22 (t, J = 6.4 Hz, 1H, H1′), 5.24 (d, J = 4.2 Hz, 1H, 3′-OH), 5.14 (t, J = 5.1 Hz, 1H, 5′-OH), 4.31−4.26 (m, 1H, H3′), 3.86 (dt, J = 3.2, 2.6 Hz, 1H, H4′), 3.71−3.59 (m, 2H, H5′), 2.23 (ddd, J = 13.0, 6.4, 3.9 Hz, 1H, H2′), 2.11 (ddd, J = 13.0, 6.4, 6.0 Hz, 1H, H2′). ^{13}C NMR (101 MHz, DMSO-d_6): δ 161.6 (C4), 153.6 (C5 furan), 152.2 (C2), 146.9 (C2 furan), 139.9 (C6), 129.9 (C1 Ph), 128.7 (C3 Ph), 127.3 (C4 Ph), 123.4 (C2 Ph), 108.9 (C4 furan), 107.4 (C3 furan), 98.0 (C5), 87.5 (C4′), 85.5 (C1′), 70.0 (C3′), 61.0 (C5′), 40.9 (C2′). HRMS-ESI$^+$: calcd for $C_{19}H_{19}N_3O_5$-H$^+$ m/z 370.1397, found m/z 370.1397.

4-*N*-(*N*,*N*-Dimethylaminomethylidenyl)-5-(5-phenylfuran-2-yl)-2′-deoxycytidine (4). To a solution of 5-(5-phenylfuran-2-yl)-2′-deoxycytidine (**3**, 250 mg, 0.68 mmol) in anhydrous DMF (5 mL) was added *N*,*N*-dimethylformamide dimethyl acetal (0.4 g, 3.4 mmol). The reaction mixture was stirred for 2 h at 55 °C, and then concentrated under reduced pressure. The residue was coevaporated with xylenes (2 × 5 mL), and the crude material was purified by flash chromatography (0−10% MeOH in CH_2Cl_2) to obtain nucleoside **4** as a yellow solid (282 mg, 0.66 mmol). Yield: 98%. R_f 0.4 (6% MeOH in CH_2Cl_2). ^{1}H NMR (400 MHz, DMSO-d_6): δ 8.74 (s, 1H, H6), 8.72 (s, 1H, CH amidine), 7.80 (d, J = 7.6 Hz, 2H, H2 Ph), 7.42 (t, J = 7.6, 2H, H3 Ph), 7.26 (t, J = 7.6 Hz, 1H, H4 Ph), 7.15 (d, J = 3.4 Hz, 1H, H4 furan), 6.99 (d, J = 3.4 Hz, 1H, H3 furan), 6.28 (t, J = 6.1 Hz, 1H, H1′), 5.30 (d, J = 4.2 Hz, 1H, 3′-OH), 5.22 (t, J = 5.3 Hz, 1H, 5′-OH), 4.33 (dt, J = 4.2, 3.4 Hz, 1H, H3′), 3.93 (q, J = 3.4 Hz, 1H, H4′), 3.75−3.69 (m, 2H,

DOI: 10.1021/acs.joc.5b01577
J. Org. Chem. 2015, 80, 9592−9602

H5′), 3.24 (s, 3H, CH_3 amidine), 3.17 (s, 3H, CH_3 amidine), 2.31 (ddd, J = 13.3, 6.1, 3.4 Hz, 1H, H2′), 2.17−2.09 (m, 1H, H2′). ^{13}C NMR (101 MHz, DMSO-d_6): δ 166.1 (C2), 158.0 (C4), 153.6 (CH amidine), 150.8 (C5 furan), 147.9 (C2 furan), 138.1 (C6), 130.2 (C1 Ph), 128.8 (C3 Ph), 127.1 (C4 Ph), 123.3 (C2 Ph), 110.8 (C4 furan), 107.6 (C3 furan), 104.9 (C5), 88.0 (C4′), 86.2 (C1′), 70.4 (C3′), 61.3 (C5′), 41.2 (C2′), 41.0 (CH_3 amidine), 35.3 (CH_3 amidine). HRMS-ESI$^+$: calcd for $C_{22}H_{24}N_4O_5$-H$^+$ m/z 425.1819, found m/z 425.1808.

5′-*O*-(4,4′-Dimethoxytrityl)-4-*N*-(*N*,*N*-dimethylaminomethylidenyl)-5-(5-phenylfuran-2-yl)-2′-deoxycytidine (5). To a solution of nucleoside **4** (280 mg, 0.66 mmol) in anhydrous pyridine (5 mL) was added DMTCl (400 mg, 1.0 mmol). The reaction mixture was stirred for 16 h at rt. The reaction mixture was concentrated under reduced pressure, coevaporated with toluene (2 × 5 mL), and purified by flash chromatography (0−5% MeOH in CH_2Cl_2) to obtain nucleoside **5** as a yellow foam (316 mg, 0.44 mmol). Yield: 66%. R_f 0.4 (4% MeOH in CH_2Cl_2). ^{1}H NMR (400 MHz, $CDCl_3$): δ 8.89 (s, 1H, H6), 8.34 (s, 1H, CH amidine), 7.44−7.36 (m, 4H, H2 Ph, DMT), 7.28−7.23 (m, 5H, H4 furan, DMT), 7.18−7.06 (m, 7H, H3 Ph, H4 Ph, DMT), 6.68−6.63 (m, 5H, DMT, H3 furan), 6.36 (t, J = 6.3 Hz, 1H, H1′), 4.33 (dt, J = 6.3, 4.0 Hz, 1H, H3′), 4.18 (q, J = 4.0 Hz, 1H, H4′), 3.64 (s, 6H, OCH_3), 3.52 (dd, J = 10.1, 4.0 Hz, 1H, H5′), 3.40 (dd, J = 10.1, 4.0 Hz, 1H, H5′), 3.22 (s, 3H, CH_3 amidine), 3.21 (s, 3H, CH_3 amidine), 2.79−2.71 (m, 1H, H2′), 2.28−2.19 (m, 1H, H2′). ^{13}C NMR (101 MHz, $CDCl_3$): δ 167.2 (C2), 158.5 (DMT), 158.4 (C4), 154.9 (C5 furan), 152.2 (C2 furan), 148.0 (DMT), 144.6 (C6), 137.2 (CH amidine), 135.8, 135.5, 130.5, 130.0, 129.8, 128.6, 128.0, 127.9, 126.8, 123.5, 113.2 (DMT, Ph), 111.4 (C4 furan), 107.0 (C5), 106.5 (C3 furan), 87.3 (C1′), 86.7 (C4′), 85.9 (DMT), 72.6 (C3′), 63.8 (C5′), 55.1 (OCH_3), 41.8 (C2′), 41.4 (CH_3 amidine), 35.6 (CH_3 amidine). HRMS-ESI$^+$: calcd for $C_{43}H_{42}N_4O_7$-H$^+$ m/z 727.3126, found m/z 727.3129.

3′-*O*-(*P*-2-Cyanoethyl-*N*,*N*-diisopropylaminophosphinyl)-5′-*O*-(4,4′-dimethoxytrityl)-4-*N*-(*N*,*N*-dimethylaminomethylidenyl)-5-(5-phenylfuran-2-yl)-2′-deoxycytidine (6). Nucleoside **5** (299 mg, 0.41 mmol) was coevaporated with anhydrous 1,2-dichloroethane (2 × 3 mL) and dissolved in anhydrous CH_2Cl_2 (3 mL). Diisopropylammonium tetrazolide (139 mg, 0.82 mmol) and 2-cyanoethyl-*N*,*N*,*N*′,*N*′-tetraisopropylphosphordiamidite (248 mg, 0.82 mmol) were added, and the reaction mixture was stirred under argon for 18 h at rt. The mixture was concentrated under reduced pressure, and the residue was purified by flash chromatography (0−5% MeOH in CH_2Cl_2) to afford a colorless oil. The oil was dissolved in CH_2Cl_2 (1 mL) and poured onto cold hexanes (100 mL). The resulting precipitate was collected by decantation to obtain nucleoside phosphoramidite **6** as a light yellow solid (268 mg, 0.29 mmol). Yield: 70%. R_f 0.35 (4% MeOH in CH_2Cl_2). ^{31}P NMR (162 MHz, $CDCl_3$): δ 148.99, 148.50. HRMS-ESI$^+$: calcd for $C_{52}H_{59}N_6O_8P$-H$^+$ m/z 927.4205, found m/z 927.4160.

3′,5′-Bis-*O*-(*tert*-butyldimethylsilyl)-5-ethynyl-2′-deoxycytidine (8). 5-Ethynyl-2′-deoxycytidine (7, 0.60 g, 2.38 mmol) was dissolved in anhydrous DMF (5 mL), and imidazole (0.73 g, 10.8 mmol) was added. The reaction mixture was stirred for 5 min, and TBSCl (0.90 g, 5.97 mmol) was added in small portions. The reaction mixture was stirred for 4 h, upon which saturated aqueous solution of $NaHCO_3$ (25 mL) was added. The mixture was extracted with CH_2Cl_2 (2 × 25 mL), and the combined organic extracts were washed with water (50 mL), dried over $MgSO_4$, and concentrated under reduced pressure. The crude product was purified by flash column chromatography (0−5% MeOH in CH_2Cl_2) to obtain nucleoside **11** as a white foam (1.14 g, 2.38 mmol). Yield: quantitative. R_f 0.4 (5% MeOH in CH_2Cl_2). ^{1}H NMR (400 MHz, $CDCl_3$): δ 8.18 (s, 1H, H6), 7.36 (br, 1H, NH), 6.25 (t, J = 6.1 Hz, 1H, H1′), 5.73 (br, 1H, NH), 4.36 (dt, J = 6.1, 4.0 Hz, 1H, H3′), 3.97−3.90 (m, 2H, H4′, H5′), 3.77 (dd, J = 11.0, 2.0 Hz, 1H, H5′), 3.31 (s, 1H, C≡CH), 2.47 (ddd, J = 13.3, 6.1, 4.2 Hz, 1H, H2′), 2.03 (dt, J = 13.3, 6.1 Hz, 1H, H2′), 0.92 (s, 9H, $SiC(CH_3)_3$), 0.88 (s, 9H, $SiC(CH_3)_3$), 0.13 (s, 3H, $SiCH_3$), 0.12 (s, 3H, $SiCH_3$), 0.07 (s, 3H, $SiCH_3$), 0.06 (s, 3H, $SiCH_3$). ^{13}C NMR (101 MHz, $CDCl_3$): δ 164.7 (C4), 154.2 (C2), 144.9 (C6), 89.4 (C≡CH), 88.0 (C4′), 86.8 (C1′), 83.7 (C≡CH), 75.6 (C5), 71.4 (C3′), 62.4 (C5′), 42.6 (C2′), 26.1, 25.7 ($SiC(CH_3)_3$), 18.5, 18.0 ($SiC(CH_3)_3$), −4.6, −4.9, −5.38, −5.41 ($SiCH_3$). HRMS-ESI$^+$: calcd for $C_{23}H_{41}N_3O_4Si_2$-Na$^+$ m/z 502.2528, found m/z 502.2534.

***N*-Phenylsydnone (9).** This material was synthesized by a known method[45] from *N*-phenylglycine. Mp 135.5−137 °C. ^{1}H NMR (400 MHz, $CDCl_3$): δ 7.76−7.72 (m, 2H, H3 Ph), 7.71−7.61 (m, 3H, H2 Ph, H4 Ph), 6.76 (s, 1H, H4 sydnone). ^{13}C NMR (101 MHz, $CDCl_3$): δ 169.0 (C5 sydnone), 134.9 (C1 Ph), 132.5 (C4 Ph), 130.3 (C2 Ph), 121.3 (C3 Ph), 93.7 (C4 sydnone). IR (KBr, cm^{-1}): ν 3128 (sp^2 C—H stretch), 1751 (C═O stretch), 1472, 1440, 1176, 1087, 948, 854, 759, 726, 683. HRMS-ESI$^+$: calcd for $C_8H_6N_2O_2$-Na$^+$ m/z 185.0321, found m/z 185.0316.

5-(1-Phenyl-1*H*-pyrazol-3-yl)-2′-deoxycytidine (10). For method A, a sealed tube was charged with 3′,5′-bis-*O*-(*tert*-butyldimethylsilyl)-5-ethynyl-2′-deoxycytidine (**8**, 53 mg, 0.11 mmol), *N*-phenylsydnone (**9**, 80 mg, 0.50 mmol), and 1,2-dichlorobenzene (5 mL). The solution was stirred at 180 °C under microwave irradiation for 4 h, upon which it was cooled, and the solvent was removed under reduced pressure. The mixture of pyrazole products was dissolved in THF (3 mL) and treated with a solution of TBAF in THF (1 M, 0.25 mL, 0.25 mmol) for 1 h at rt. The solvent was evaporated, and the two regioisomers were separated by flash chromatography (0−15% MeOH in CH_2Cl_2). Nucleoside **10** was obtained in the first fraction as a white solid (12 mg; 32 μmol). Yield: 29%. R_f 0.4 (10% MeOH in CH_2Cl_2). ^{1}H NMR (400 MHz, DMSO-d_6): δ 8.71 (s, 1H, H6), 8.60 (d, J = 2.5 Hz, 1H, H5 pyrazole), 8.14 (br, 1H, NH), 7.88 (br, 1H, NH), 7.87 (d, J = 7.7 Hz, 2H, H2 Ph), 7.52 (t, J = 7.7 Hz, 2H, H3 Ph), 7.32 (t, J = 7.7 Hz, 1H, H4 Ph), 6.84 (d, J = 2.5 Hz, 1H, H4 pyrazole), 6.21 (t, J = 6.2 Hz, 1H, H1′), 5.36 (t, J = 4.9 Hz, 1H, 5′-OH), 5.24 (d, J = 4.4 Hz, 1H, 3′-OH), 4.34−4.27 (m, 1H, H3′), 3.89−3.83 (m, 1H, H4′), 3.80−3.72 (m, 1H, H5′), 3.70−3.63 (m, 1H, H5′), 2.24 (ddd, J = 4.6, 6.3, 13.2, 1H, H2′), 2.18−2.10 (m, 1H, H2′). ^{13}C NMR (101 MHz, DMSO-d_6): δ 162.1 (C4), 153.5 (C2), 148.2 (C3 pyrazole), 140.5 (C6), 139.0 (C1 Ph), 129.5 (C3 Ph), 128.9 (C5 pyrazole), 126.1 (C4 Ph), 118.0 (C2 Ph), 104.2 (C4 pyrazole), 98.3 (C5), 87.3 (C4′), 85.4 (C1′), 69.4 (C3′), 60.6 (C5′), 41.0 (C2′). HRMS-ESI$^+$: calcd for $C_{18}H_{19}N_5O_4$-H$^+$ m/z 370.1510, found m/z 370.1512. The corresponding 1,4-substituted pyrazole isomer (5-(1-phenyl-1*H*-pyrazol-4-yl)-2′-deoxycytidine) was obtained in the second fraction as a white solid (6.0 mg; 16 μmol). Yield: 15%. R_f 0.35 (10% MeOH in CH_2Cl_2). ^{1}H NMR (400 MHz, DMSO-d_6): δ 8.57 (s, 1H, H6), 8.07 (s, 1H, H3 pyrazole), 7.88 (d, J = 8.5, 2H, Ph), 7.82 (s, 1H, H5 pyrazole), 7.52 (t, J = 8.5, 2H, Ph), 7.32 (t, J = 8.5, 1H, Ph), 6.22 (t, J = 6.5 Hz, 1H, H1′), 4.27 (dt, J = 7.3, 3.7 Hz, 1H, H3′), 3.79 (q, J = 3.5 Hz, 1H, H4′), 3.63 (dd, J = 11.8, 3.5 Hz, 1H, H5′), 3.59 (dd, J = 11.8, 3.5 Hz, 1H, H5′), 2.22−2.05 (m, 2H, H2′). ^{13}C NMR (400 MHz, DMSO-d_6): δ 163.4 (C4), 154.3 (C2), 140.1 (C3 pyrazole), 139.52 (C3 pyrazole), 139.48 (C1 Ph), 129.4 (C3 Ph), 126.3 (C4 Ph), 126.2 (C6), 118.4 (C2 Ph), 115.7 (C4 pyrazole), 98.4 (C5), 87.2 (C4′), 85.0 (C1′), 69.8 (C3′), 60.8 (C5′), 40.6 (C2′). HRMS-ESI$^+$: calcd for $C_{18}H_{19}N_5O_4$-H$^+$ m/z 370.1510, found m/z 370.1510. For method B, to a degassed solution of 5-iodo-2′-deoxycytidine (**1**, 250 mg, 0.71 mmol) and 1-phenyl-1*H*-pyrazol-3-boronic acid MIDA ester (**12**, 303 mg, 1.01 mmol) in DMF:H_2O (7:1, 15 mL) were added K_3PO_4 (300 mg, 1.42 mmol) and $Pd(PPh_3)_4$ (164 mg, 0.14 mmol). The mixture was stirred at 60 °C for 48 h, and then concentrated under reduced pressure and purified by flash chromatography (0−10% MeOH in CH_2Cl_2) to obtain nucleoside **9** as a white solid (210 mg; 0.57 mmol). Yield: 80%.

1-Phenyl-1*H*-pyrazol-3-boronic Acid MIDA Ester (12). *N*-Phenylsydnone (**9**, 1.0 g, 6.17 mmol) and commercial ethynylboronic acid MIDA ester (**11**, 1.34 g, 7.40 mmol) were suspended in anhydrous anisole (25 mL) in a 50 mL steel bomb. The reaction chamber was heated to 165 °C in an oven for 36 h, and slowly cooled to rt. The reaction mixture was filtered, and the filtrate was concentrated under reduced pressure; the two regioisomers were separated by flash chromatography (50−100% EtOAc in hexanes). Compound **12** was obtained in the first fraction as a light brown solid (0.98 g; 3.27 mmol). Yield: 53%. R_f 0.5 (5% MeOH in CH_2Cl_2). ^{1}H NMR (400 MHz, DMSO-d_6): δ 8.46 (d, J = 2.4 Hz, 1H, H5 pyrazole), 7.86 (d, J = 7.5 Hz, 2H, H2 Ph), 7.49 (t, J = 7.5 Hz, 2H, H3 Ph), 7.29 (t, J = 7.5 Hz, 1H, H4

DOI: 10.1021/acs.joc.5b01577
J. Org. Chem. 2015, 80, 9592−9602

Ph), 6.58 (d, J = 2.4 Hz, 1H, H4 pyrazole), 4.36 (d, J = 17.1 Hz, 2H, CH_2), 4.11 (d, J = 17.1 Hz, 2H, CH_2), 2.65 (s, 3H, CH_3). ^{13}C NMR (101 MHz, DMSO-d_6): δ 169.2 (C═O), 139.8 (C1 Ph), 129.4 (C3 Ph), 127.7 (C5 pyrazole), 126.1 (C4 Ph), 118.6 (C2 Ph), 112.7 (C4 pyrazole), 104.4 (C3 pyrazole), 61.4 (CH_2), 47.3 (CH_3). HRMS-ESI$^+$: calcd for $C_{14}H_{14}BN_3O_4$-H$^+$ m/z 300.1153, found m/z 300.1157. The corresponding 1,4-substituted pyrazole isomer was obtained in the second fraction as a light brown solid (0.34 g; 1.14 mmol). Yield: 19%. R_f 0.45 (5% MeOH in CH_2Cl_2). ^{1}H NMR (400 MHz, DMSO-d_6): δ 8.40 (s, 1H, H5 pyrazole), 7.86 (d, J = 7.8 Hz, 2H, Ph), 7.71 (s, 1H, H3 pyrazole), 7.49 (t, J = 7.8 Hz, 2H, Ph), 7.29 (t, J = 7.8 Hz, 1H, Ph), 4.33 (d, J = 17.1 Hz, 2H, CH_2), 4.11 (d, J = 17.1 Hz, 2H, CH_2), 2.67 (s, 3H, CH_3). ^{13}C NMR (400 MHz, DMSO-d_6): δ 169.0 (C═O), 144.8 (C3 pyrazole), 139.6 (C1 Ph), 131.4 (C5 pyrazole), 129.4 (C3 Ph), 125.9 (C4 Ph), 118.3 (C2 Ph), 99.4 (C4 pyrazole), 61.2 (CH_2), 47.3 (CH_3). HRMS-ESI$^+$: calcd for $C_{14}H_{14}BN_3O_4$-H$^+$ m/z 300.1153, found m/z 300.1150.

5′-*O*-(4,4′-Dimethoxytrityl)-5-(1-phenyl-1*H*-pyrazol-3-yl)-2′-deoxycytidine (13). To a solution of nucleoside **10** (326 mg; 0.88 mmol) in anhydrous pyridine (5 mL) was added DMTCl (419 mg; 1.24 mmol). The mixture was stirred at rt for 16 h, and then concentrated under reduced pressure. The residue was purified by flash chromatography (0−6% MeOH in CH_2Cl_2) to obtain unreacted nucleoside **10** as a white solid (169 mg; 0.46 mmol) and nucleoside **13** as a light yellow foam (224 mg; 0.33 mmol). Yield: 38%. R_f 0.5 (5% MeOH in CH_2Cl_2). ^{1}H NMR (400 MHz, $CDCl_3$): δ 8.51 (br, 1H, NH), 8.21 (s, 1H, H6), 7.57 (d, J = 7.6 Hz, 2H, H2 Ph), 7.54 (d, J = 2.5 Hz, 1H, H5 pyrazole), 7.48−7.39 (m, 4H, H3 Ph, DMT), 7.34−7.21 (m, 8H, DMT), 7.20−7.14 (m, 1H, H4 Ph), 6.77 (d, J = 8.0 Hz, 4H, DMT), 6.61 (br, 1H, NH), 6.51 (t, J = 6.5 Hz, 1H, H1′), 5.87 (d, J = 2.5 Hz, 1H, H4 pyrazole), 4.54−4.47 (m, 1H, H3′), 4.29−4.21 (m, 1H, H4′), 3.71 (s, 6H, DMT), 3.50 (dd, J = 10.4, 3.2 Hz, 1H, H5′), 3.30 (dd, J = 10.4, 4.0 Hz, 1H, H5′), 2.92−2.81 (m, 1H, H2′), 2.23 (dt, J = 13.3, 6.5 Hz, 1H, H2′). ^{13}C NMR (101 MHz, $CDCl_3$): δ 162.8 (C4), 158.6 (DMT), 155.0 (C2), 147.9 (DMT), 144.5 (C3 pyrazole), 139.5 (C1 Ph), 138.8 (C6), 135.7, 135.6, 130.1, 129.5, 128.2, 128.0 (DMT, C3 Ph), 127.5 (C5 pyrazole), 127.0 (C4 Ph), 126.6 (DMT), 118.7 (C2 Ph), 113.2 (DMT), 104.2 (C4 pyrazole), 100.0 (C5), 86.8 (DMT), 86.6 (C4′), 86.2 (C1′), 71.9 (C3′), 63.7 (C5′), 55.19 (DMT), 42.3 (C2′). HRMS-ESI$^+$: calcd for $C_{39}H_{37}N_5O_6$-Na$^+$ m/z 694.2636, found m/z 694.2617.

3′-*O*-(*P*-2-Cyanoethyl-*N*,*N*-diisopropylaminophosphinyl)-5′-*O*-(4,4′-dimethoxytrityl)-5-(1-phenyl-1*H*-pyrazol-3-yl)-2′-deoxycytidine (14). Compound **13** (242 mg, 0.36 mmol) was coevaporated with anhydrous 1,2-dichloroethane (2 × 3 mL) and dissolved in anhydrous CH_2Cl_2 (2.5 mL). Diisopropylammonium tetrazolide (122 mg, 0.72 mmol) and 2-cyanoethyl-*N*,*N*,*N*′,*N*′-tetraisopropylphosphordiamidite (217 mg, 0.72 mmol) were added, and the reaction mixture was stirred under argon for 18 h. The mixture was concentrated under reduced pressure and purified by flash chromatography (0−5% MeOH in CH_2Cl_2) to afford a colorless oil. The oil was dissolved in CH_2Cl_2 (1 mL) and poured onto cold hexanes (100 mL). The resulting precipitate was decanted and washed with cold hexanes (50 mL) to obtain nucleoside phosphoramidite **14** as a white solid (200 mg, 0.23 mmol). Yield: 64%. R_f 0.5 (3% MeOH in CH_2Cl_2). ^{31}P NMR (162 MHz, $CDCl_3$): δ 149.18, 148.47. HRMS-ESI$^+$: calcd for $C_{48}H_{54}N_7O_7P$−H$^+$ m/z 872.3895, found m/z 872.3855.

5-(1-Phenyl-1*H*-pyrazol-3-yl)-2′-deoxyuridine (17). To a stirred solution of 5-ethynyl-2′-deoxyuridine (**15**, 365 mg; 1.45 mmol) in anhydrous DMF (5 mL) was added imidazole (443 mg; 6.5 mmol). After 5 min, TBSCl (0.55 g; 3.62 mmol) was added in portions, and the reaction mixture was stirred for 4 h at rt. A saturated aqueous solution of $NaHCO_3$ (25 mL) was added, and the mixture was extracted with CH_2Cl_2 (2 × 25 mL). The combined organic phases were washed with water (50 mL), dried over $MgSO_4$, and concentrated under reduced pressure to obtain nucleoside **16** as a white foam (695 mg; 1.45 mmol). Yield: quantitative. R_f 0.65 (5% MeOH in CH_2Cl_2). ^{1}H NMR (400 MHz, $CDCl_3$): δ 8.39 (br, 1H, NH), 8.10 (s, 1H, H6), 6.29 (dd, J = 7.4, 5.9 Hz, 1H, H1′), 4.41 (dt, J = 5.5, 2.5 Hz, 1H, H3′), 3.98 (q, J = 2.5 Hz, 1H, H4′), 3.91 (dd, J = 11.5, 2.5 Hz, 1H, H5′), 3.77 (dd, J = 11.5, 2.5 Hz, 1H, H5′), 3.17 (s, 1H, C≡CH), 2.33 (ddd, J = 13.2, 5.9, 5.5 Hz, 1H, H2′), 2.03 (ddd, J = 13.2, 7.4, 5.5 Hz, 1H, H2′), 0.93 (s, 9H, $SiC(CH_3)_3$), 0.90 (s, 9H, $SiC(CH_3)_3$), 0.14 (s, 3H, $SiCH_3$), 0.13 (s, 3H, $SiCH_3$), 0.09 (s, 3H, $SiCH_3$), 0.08 (s, 3H, $SiCH_3$). ^{13}C NMR (101 MHz, $CDCl_3$): δ 161.2 (C4), 149.0 (C2), 143.7 (C6), 99.0 (C5), 88.5 (C4′), 85.9 (C1′), 82.2 (C≡CH), 74.8 (C≡CH), 72.3 (C3′), 62.9 (C5′), 42.2 (C2′), 26.1, 25.7 ($SiC(CH_3)_3$), 18.5, 18.0 ($SiC(CH_3)_3$), −4.6, −4.8, −5.3, −5.4 ($SiCH_3$). HRMS-ESI: calcd for $C_{23}H_{40}N_2O_5Si_2$-Na$^+$ m/z 503.2368, found m/z 503.2352. To a solution of 3′,5′-bis-*O*-(*tert*-butyldimethylsilyl)-5-ethynyl-2′-deoxyuridine (**16**, 670 mg, 1.39 mmol) in 1,2-dichlorobenzene (15 mL) was added *N*-phenylsydnone (260 mg, 1.60 mmol). The mixture was stirred under microwave irradiation for 5 h at 200 °C, and the black solution was concentrated under reduced pressure. The residue was purified by flash chromatography (0−80% EtOAc in hexanes) to obtain an inseparable mixture of the two pyrazole isomers (about 4:1 ratio by ^{1}H NMR) as a yellow solid (441.2 mg, 0.74 mmol). Yield: 53%. R_f 0.65 (3% MeOH in CH_2Cl_2). The mixture of two regioisomers (422 mg, 0.70 mmol) was dissolved in THF (5 mL), and TBAF (1 M solution in THF; 0.77 mL, 0.77 mmol) was added. The reaction mixture was stirred for 1 h and concentrated under reduced pressure. The residue was purified by flash chromatography (0−6% MeOH in CH_2Cl_2). Nucleoside **17** was obtained in the first fraction as a white solid (199 mg, 0.54 mmol). Yield: 77%. R_f 0.25 (5% MeOH in CH_2Cl_2). ^{1}H NMR (400 MHz, DMSO-d_6, **17**): δ 11.58 (br, 1H, NH), 8.60 (s, 1H, H6), 8.50 (d, J = 2.5 Hz, 1H, H5 pyrazole), 7.90 (dt, J = 8.5, 1.0 Hz, 2H, H2 Ph), 7.50 (ddd, J = 8.5, 7.5, 2.0 Hz, 2H, H3 Ph), 7.30 (tt, J = 7.5 Hz, 1.0 Hz, H4 Ph), 6.96 (d, J = 2.5 Hz, 1H, H4 pyrazole), 6.25 (t, J = 6.7 Hz, 1H, H1′), 5.29 (d, J = 4.2 Hz, 1H, 3′-OH), 5.07 (t, J = 5.1 Hz, 1H, 5′−OH), 4.33−4.29 (m, 1H, H3′), 3.86 (q, J = 3.5 Hz, 1H, H4′), 3.65−3.62 (m, 2H, H5′), 2.23−2.19 (m, 2H, H2′). ^{13}C NMR (101 MHz, DMSO-d_6, **17**): δ 161.5 (C4), 149.7 (C2), 145.5 (C3 pyrazole), 139.4 (C1 Ph), 137.1 (C6), 129.4 (C3 Ph), 128.0 (C4 Ph), 126.0 (C5 pyrazole), 118.1 (C2 Ph), 107.6 (C5), 106.6 (C4 pyrazole), 87.6 (C4′), 84.6 (C1′), 70.4 (C3′), 61.2 (C5′), 40.0 (C2′). The corresponding 1,4-substituted pyrazole isomer (5-(1-phenyl-1*H*-pyrazol-4-yl)-2′-deoxyuridine) was obtained in the second fraction as a white solid (18 mg, 0.05 mmol). Yield: 7%. R_f 0.20 (5% MeOH in CH_2Cl_2). ^{1}H NMR (400 MHz, $CDCl_3$): δ 11.57 (br, 1H, NH), 8.68 (d, J = 0.1 Hz, 1H, H3 pyrazole), 8.47 (s, 1H, H6), 8.06 (d, J = 0.1 Hz, 1H, H5 pyrazole), 7.82 (dd, J = 8.5, 1.0 Hz, 2H, H2 Ph), 7.54−7.48 (m, 2H, H3 Ph), 7.32 (tt, J = 7.5, 1.0 Hz, 1H, H4 Ph), 6.23 (t, J = 6.7 Hz, 1H, H1′), 5.36 (t, J = 4.8 Hz, 1H, 5′-OH), 5.29 (d, J = 4.3 Hz, 1H, 3′-OH), 4.36−4.31 (m, 1H, H3′), 3.84 (q, J = 3.3 Hz, 1H, H4′), 3.73 (ddd, J = 11.8, 4.8, 3.3 Hz, 1H, H5′), 3.66 (ddd, J = 11.8, 4.4, 3.4 Hz, 1H, H5′), 2.27 (dt, J = 12.8, 6.3 Hz, 1H, H2′), 2.18 (ddd, J = 12.8, 6.7, 4.0 Hz, 1H, H2′). ^{13}C NMR (101 MHz, DMSO-d_6): δ 161.6 (C4), 149.5 (C2), 139.4 (C1 Ph), 138.4 (C5 pyrazole), 135.3 (C6), 129.5 (C3 Ph), 126.2 (C4 Ph), 124.4 (C3 pyrazole), 118.2 (C2 Ph), 116.1 (C4 pyrazole), 105.6 (C5), 87.4 (C4′), 84.4 (C1′), 69.7 (C3′), 60.7 (C5′), 39.9 (C2′). HRMS-ESI: calcd for $C_{18}H_{18}N_4O_5$-H$^+$ m/z 371.1350, found m/z 371.1352.

3′-*O*-(*P*-2-Cyanoethyl-*N*,*N*-diisopropylaminophosphinyl)-5′-*O*-(4,4′-dimethoxytrityl)-5-(1-phenyl-1*H*-1,2,3-triazol-4-yl)-2′-deoxyuridine. To a solution of 5-ethynyl-2′-deoxyuridine (**15**, 498 mg, 1.97 mmol) in anhydrous pyridine (8 mL) was slowly added DMTCl (0.80 g; 2.37 mmol). The reaction mixture was stirred for 16 h at rt, quenched with MeOH (1 mL), and then concentrated under reduced pressure. The crude material was coevaporated with toluene (2 × 10 mL), and purified by flash chromatography (0−5% MeOH in CH_2Cl_2) to obtain 5′-*O*-(4,4′-dimethoxytrityl)-5-ethynyl-2′-deoxyuridine as a white foam (1.04 g; 1.88 mmol). Yield: 95%. R_f 0.35 (5% MeOH in CH_2Cl_2). ^{1}H NMR (400 MHz, DMSO-d_6): δ 11.72 (br, 1H, NH), 7.96 (s, 1H, H6), 6.10 (t, J = 6.7 Hz, 1H, H1′), 5.34 (d, J = 4.8 Hz, 1H, 3′-OH), 4.25 (td, J = 4.8, 3.7 Hz, 1H, H3′), 3.99 (s, 1H, C≡CH), 3.93−3.89 (m, 1H, H4′), 3.74 (s, 6H, DMT), 3.24 (dd, J = 10.5, 5.4 Hz, 1H, H5′), 3.12 (dd, J = 10.5, 2.7 Hz, 1H, H5′), 2.30−2.24 (m, 1H, H2′), 2.19 (ddd, J = 13.5, 6.7, 3.7 Hz, 1H, H2′). ^{13}C NMR (101 MHz, DMSO-d_6): δ 161.6 (C4), 158.0 (DMT), 149.3 (C2), 144.8 (C6), 143.9, 135.5, 135.3, 129.7, 129.7, 127.9, 127.6, 126.7, 113.2 (DMT), 97.8 (C5), 85.8 (C4′), 85.0 (C1′), 83.7 (C≡CH), 75.8 (C≡

DOI: 10.1021/acs.joc.5b01577
J. Org. Chem. 2015, 80, 9592−9602

CH), 70.3 (C3′), 63.7 (C5′), 55.0 (DMT), 40.0 (C2′). HRMS-ESI: calcd for $C_{32}H_{30}N_2O_7$-Na^+ m/z 577.1945, found m/z 577.1949. A microwave vial was charged with 5′-*O*-(4,4′-dimethoxytrityl)-5-ethynyl-2′-deoxyuridine (450 mg, 0.81 mmol) and H_2O/*t*-BuOH/pyridine (2:2:1, 15 mL). Sodium ascorbate (96 mg, 0.49 mmol), $CuSO_4 \cdot 5H_2O$ (40 mg, 0.17 mmol), and azidobenzene (3.25 mL, 1.62 mmol) were added, and the reaction mixture was stirred for 1 h at 100 °C using microwave irradiation. The reaction mixture was concentrated under reduced pressure and purified by flash chromatography (0−10% MeOH in CH_2Cl_2) to obtain 5′-*O*-(4,4′-dimethoxytrityl)-5-(1-phenyl-1*H*-1,2,3-triazol-4-yl)-2′-deoxyuridine as a white foam (297 mg, 0.44 mmol). Yield: 73%. R_f 0.75 (5% MeOH in CH_2Cl_2). ^{1}H NMR (400 MHz, DMSO-d_6): δ 11.81 (s, 1H, NH), 8.82 (s, 1H, H6), 8.40 (s, 1H, CH triazole), 7.91 (d, J = 7.5 Hz, 2H, H2 Ph), 7.60 (t, J = 7.5 Hz, 2H, H3 Ph), 7.50 (t, J = 7.5 Hz, 1H, H4 Ph), 7.37 (d, J = 7.3 Hz, 2H, DMT), 7.31−7.20 (m, 4H, DMT), 7.20−7.10 (m, 3H, DMT), 6.82 (dd, J = 9.0, 2.0 Hz, 4H, DMT), 6.20 (t, J = 6.4 Hz, 1H, H1′), 5.36 (d, J = 6.8 Hz, 1H, 3′-OH), 4.21 (dt, J = 6.2, 4.2 Hz, 1H, H3′), 3.96 (q, J = 4.2 Hz, 1H, H4′), 3.67 (s, 3H, DMT), 3.66 (s, 3H, DMT), 3.25−3.19 (m, 2H, H5′), 2.30−2.24 (m, 2H, H2′). ^{13}C NMR (101 MHz, DMSO-d_6): δ 161.1 (C4), 158.0 (C2), 149.6 (DMT), 144.8 (DMT), 139.8 (C1 Ph), 136.3 (C5 triazole), 135.5 (DMT), 135.4 (DMT), 129.9 (C3 Ph), 129.7 (DMT), 129.6 (C4 Ph), 127.8 (DMT), 127.6 (DMT), 126.6 (DMT), 120.1 (C2 Ph), 113.1 (DMT), 85.75 (C4′), 85.74 (C1′), 70.4 (C3′), 63.6 (C5′), 54.9 (DMT), 39.6 (C2′). HRMS-ESI: calcd for $C_{38}H_{35}N_5O_7$-Na^+ m/z 696.2429, found m/z 696.2417. 5′-*O*-(4,4′-Dimethoxytrityl)-5-(1-phenyl-1*H*-1,2,3-triazol-4-yl)-2′-deoxyuridine (205 mg, 0.30 mmol) was coevaporated with anhydrous 1,2-dichloroethane (2 × 3 mL) and dissolved in anhydrous CH_2Cl_2 (3 mL). Diisopropylammonium tetrazolide (121.3 mg, 0.6 mmol) and 2-cyano-*N*,*N*,*N*′,*N*′-tetraisopropylphosphordiamidite (183.4 mg; 0.6 mmol) were added, and the reaction mixture was stirred under argon for 18 h. The mixture was concentrated under reduced pressure and purified by flash chromatography (0−5% MeOH in CH_2Cl_2) to afford crude material, which was dissolved in CH_2Cl_2 (1 mL) and poured onto cold hexanes (100 mL). The resulting precipitate was collected by decantation to obtain 3′-*O*-(*P*-2-cyanoethyl-*N*,*N*-diisopropylamino-phosphinyl)-5′-*O*-(4,4′-dimethoxytrityl)-5-(1-phenyl-1*H*-1,2,3-triazol-4-yl)-2′-deoxyuridine as a white solid (192.4 mg, 0.22 mmol). Yield: 73%. R_f 0.5 (5% MeOH in CH_2Cl_2). ^{31}P NMR (162 MHz, $CDCl_3$): δ 149.19, 148.74. HRMS-ESI: calcd for $C_{47}H_{52}N_7O_8P$-Na^+ m/z 896.3507, found m/z 896.3478.

Oligonucleotides. Oligonucleotides were synthesized on a fully automated DNA synthesizer in ∼0.2 μmol scale loaded on 500 Å controlled-pore glass (CPG) supports using the phosphoramidite approach and following the manufacturer's protocol. Double coupling (2 × 5 min) cycles were used for commercial phosphoramidites, and prolonged coupling times (20 min) were used for the modified phosphoramidites **6** and **14**. The phosphoramidites were activated using 1*H*-tetrazole for **6** or HOBt for **14**, and incorporated into oligonucleotides via manual couplings: 10 μmol of the modified phosphoramidite was dissolved in anhydrous MeCN (2 mL) and treated with either 1*H*-tetrazole (3 mL, 0.45 M solution in MeCN) or HOBt (3 mL, 0.3 M solution in 15:1 v/v MeCN/DMF) for **6** and **14**, respectively, and infused into the reaction compartment. The stepwise coupling efficiencies were monitored by measuring the absorbance of the trityl cation at 495 nm, which in all cases was 98−100% for the commercial phosphoramidites, and 92−100% for the modified phosphoramidites. The final 5′-terminal DMT group in the oligonucleotides was kept on for purification purposes. The final crude oligonucleotides on solid support were treated with NH_3 (28% in H_2O, 1 mL) at 55 °C for 16 h. The mixture was filtered, and the filtrate was evaporated to dryness at 45 °C by a steady N_2 flow, and dissolved in an aqueous triethylammonium acetate buffer (500 μL, 0.05 M, pH 7.4). The oligonucleotides were purified by reversed-phase HPLC on a Waters 600 system using Xterra MS C18 10 μm (7.8 mm × 50 mm) columns and Xterra MS C18 10 μm (7.8 mm × 10 mm) precolumns. Elution was performed with 100% eluent A over 2 min, followed by a linear gradient down to 30% eluent A over 38 min, then a wash with 100% eluent B over 10 min, 100% eluent A over 10 min (eluent A = triethylammonium acetate (0.05 M, pH 7.4); eluent B = 75% MeCN/H_2O (3:1, v/v)). The pure fractions were pooled and evaporated at 45 °C. The 5′-terminal DMT group was removed by treatment with acetic acid (80% in H_2O, 100 μL) for 30 min, upon which an aqueous solution of NaOAc (15 μL, 3 M), an aqueous solution of $NaClO_4$ (15 μL, 5 M), and pure acetone (1 mL) were added. The oligonucleotides precipitated overnight at −20 °C. The supernatant was removed from the sedimented solid (centrifugation, 12 000 rpm, 10 min at 2 °C), and the remaining pellet was washed with cold acetone (3 × 1 mL) and dissolved in 500 μL of pure water. Analytically pure oligonucleotides were obtained by preparative anion-exchange HPLC (IE-HPLC) using a DIONEX Ultimate 3000 system equipped with DNAPac PA100 semipreparative columns (13 μm, 250 mm × 9 mm) heated to 60 °C. Elution was performed with an isocratic hold of 10% eluent B, starting from 2 min hold on 2% eluent A in pure water, followed by a linear gradient to 25% eluent A in 20 min at a flow rate of 2.0 mL/min (eluent A = $NaClO_4$ (1.0 M); eluent B = TrisCl (0.25 M), pH 8.0). The pure fractions were desalted using NAP-5 or NAP-10 Sephadex columns according to the manufacturer's instructions, and evaporated at 45 °C. Mass spectra of the oligonucleotides were recorded on a MALDI-TOF MS instrument in ES^+ mode. Analytical IE-HPLC traces were recorded on a Merck-Hitachi Lachrom system equipped with a DNAPac PA100 analytical column (13 μm, 250 mm × 4 mm). The concentrations of the purified oligonucleotides were determined by the optical density at 260 nm, assuming that the molar absorptivities of the oligonucleotides equal the sum of each constituent nucleotide monomers. The extinction coefficients of the modified monomers in mL μmol^{-1} cm^{-1}, ε_{260} (**W**) = 7.8, ε_{260} (**Y**) = 9.7, and ε_{260} (**Z**) = 14.6, were determined from the slopes of the absorbance of the fully deprotected nucleosides at 25, 50, 75, and 100 μM concentrations ($R^2 > 0.9995$).

Melting Temperatures. The duplex samples consisted of 1.5 μM concentrations of each oligonucleotide in medium salt buffer [Na_2HPO_4 (2.5 mM), NaH_2PO_4 (5 mM), NaCl (100 mM), EDTA (0.1 mM), pH 7]. The strands were annealed by heating the sample to 80 °C followed by a slow cooling to 10 °C. The increase in absorbance at 260 nm as a function of temperature from 10 to 75 °C or 80 °C (1 °C/min) was recorded on a UV−vis spectrometer using a Peltier Temperature Programmer. The listed T_m values are averages of at least duplicate readings within 0.5 °C, as determined from the local maximum of the first derivatives of the absorbance versus temperature curves. All melting curves were found to be reversible.

Circular Dichroism. CD spectra were recorded at 20 °C on a CD spectrometer as an average of 5 scans from 200−350 nm using a split of 2.0 nm, and a scan speed of 50 nm/min. The samples were prepared similarly to the samples used for the melting temperature studies with 1.5 μM concentrations of each strand. Quartz optical cells with a path length of 5.0 mm were used.

Molecular Dynamics Simulations. The global minimum structures were found from 5 ns molecular dynamics simulations using the all-atom AMBER* force field applying the GB/SA solvation model[46] with extended cut-offs for nonbonded interactions (van der Waals 8 Å and electrostatics 20 Å). Calculations were performed in MacroModel V10.4 (within Maestro V9.8.017). The hybrid duplexes were built in B-type helical geometries, and relaxed with AMBER*. Initial Monte Carlo torsional samplings (MCMM) were performed to generate 1000 structures, which were minimized into local minima. The lowest energy structures of each simulations were used for the subsequent MD simulations. The MD simulations were performed at 300 K. SHAKE all bonds to hydrogen was imposed in order to increase the time step to 2.2 fs, and an equilibrium time of 100 ps was used to stabilize the calculations. A multiple minimization of the 500 sampled structures was performed to obtain a converged global minimum structure.

***Ab Initio* Calculations.** The torsional energy profiles were calculated on the geometry optimized structures by a series of fully relaxed coordinate scans of the dihedral angles between the nucleobases and the 5-substituents in vacuum. The computations were performed in Jaguar V7.8 (within Maestro V9.8.017) at the local MP2 level with the 6-31G** basis set, and by applying the Pipek−Mezey valence

DOI: 10.1021/acs.joc.5b01577
J. Org. Chem. 2015, 80, 9592−9602

localization method.[47] The torsional sampling was performed by 2° increments of the dihedral angles (from 0° to 360°) to obtain 181 structures, the relative energies of which were plotted against the corresponding torsion angle.

■ ASSOCIATED CONTENT

Supporting Information

The Supporting Information is available free of charge on the ACS Publications website at DOI: 10.1021/acs.joc.5b01577.

Dihedral scan curves of the eight model compounds, melting temperatures of DNA:DNA duplexes, optimized synthesis of the phosphoramidite of monomer **W**, selected NMR spectra, MALDI-TOF data of oligonucleotides, analytical IE-HPLC profiles of oligonucleotides, thermal denaturation curves, and top views of the minimized duplex structures (PDF)

■ AUTHOR INFORMATION

Corresponding Author

*E-mail: pouln@sdu.dk.

Notes

The authors declare no competing financial interest.

■ ACKNOWLEDGMENTS

The project was supported by The Danish Council for Independent Research | Natural Sciences (FNU), and the Villum Kann Rasmussen Fonden.

■ REFERENCES

(1) O'Connor, L.; Glynn, B. *Expert Rev. Med. Devices* **2010**, *7*, 529−539.
(2) Kurreck, J. *Therapeutic Oligonucleotides*; Royal Society of Chemistry: London, U.K., 2008.
(3) Goodchild. *Methods Mol. Biol.* **2011**, *764*, 1−15.
(4) Castanotto, D.; Rossi, J. J. *Nature* **2009**, *457*, 426−433.
(5) Dias, N.; Stein, C. A. *Mol. Cancer Ther.* **2002**, *1*, 347−355.
(6) Aartsma-Rus, A.; van Ommen, G.-J. B. *RNA* **2007**, *13*, 1609−1624.
(7) Riboldi, G.; Zanetta, C.; Ranieri, M.; Nizzardo, M.; Simone, C.; Magri, F.; Bresolin, N.; Comi, G. P.; Corti. *Mol. Neurobiol.* **2014**, *50*, 721−732.
(8) Gleave, M. E.; Monia, B. P. *Nat. Rev. Cancer* **2005**, *5*, 468−479.
(9) Devi, G. R. *Cancer Gene Ther.* **2006**, *13*, 819−829.
(10) Spurgers, K. B.; Sharkey, C. M.; Warfield, K. L.; Bavari, S. *Antiviral Res.* **2008**, *78*, 26−36.
(11) Deleavey, G. F.; Damha, M. *Chem. Biol.* **2012**, *19*, 937−954.
(12) Watts, J. K.; Corey, D. R. *J. Pathol.* **2012**, *226*, 365−379.
(13) Singh, S. K.; Nielsen, P.; Koshkin, A. A.; Wengel, J. *Chem. Commun.* **1998**, *4*, 455−456.
(14) Obika, S.; Nanbu, D.; Hari, Y.; Andoh, J.; Morio, K.; Doi, T.; Imanishi, T. *Tetrahedron Lett.* **1998**, *39*, 5401−5404.
(15) Karkare, S.; Bhatnagar, D. *Appl. Microbiol. Biotechnol.* **2006**, *71*, 575−586.
(16) Zhang, L.-H.; Xi, Z.; Chattopadhyaya, J. *Medicinal Chemistry of Nucleic Acids*; John Wiley & Sons: New York, 2011.
(17) Petersheim, M.; Turner, D. H. *Biochemistry* **1983**, *22*, 256−263.
(18) Yakovchuk, P.; Protozanova, E.; Frank-Kamenetskii, M. D. *Nucleic Acids Res.* **2006**, *34*, 564−574.
(19) Luyten, I.; Herdewijn, P. *Eur. J. Med. Chem.* **1998**, *33*, 515−576.
(20) Lin, K.-Y.; Jones, R. J.; Matteucci, M. D. *J. Am. Chem. Soc.* **1995**, *117*, 3873−3874.
(21) Gutierrez, A. J.; Terhorst, T. J.; Matteucci, M. D.; Froehler, B. C. *J. Am. Chem. Soc.* **1994**, *116*, 5540−5544.
(22) Ahmadian, M.; Bergstrom, D. E. In *Modified Nucleosides*; Herdewijn, P., Ed.; Wiley-VCH Verlag GmbH & Co. KGaA: Berlin, 2008; pp 249−276.
(23) Kočalka, P.; Andersen, N. K.; Jensen, F.; Nielsen, P. *ChemBioChem* **2007**, *8*, 2106−2116.
(24) Andersen, N. K.; Chandak, N.; Brulíková, L.; Kumar, P.; Jensen, M. D.; Jensen, F.; Sharma, P. K.; Nielsen, P. *Bioorg. Med. Chem.* **2010**, *18*, 4702−4710.
(25) Andersen, N. K.; Døssing, H.; Jensen, F.; Vester, B.; Nielsen, P. *J. Org. Chem.* **2011**, *76*, 6177−6187.
(26) Kumar, P.; Chandak, N.; Nielsen, P.; Sharma, P. K. *Bioorg. Med. Chem.* **2012**, *20*, 3843−3849.
(27) Kumar, P.; Hornum, M.; Nielsen, L. J.; Enderlin, G.; Andersen, N. K.; Len, C.; Hervé, G.; Sartori, G.; Nielsen, P. *J. Org. Chem.* **2014**, *79*, 2854−2863.
(28) Kaura, M.; Kumar, P.; Hrdlicka, P. J. *Org. Biomol. Chem.* **2012**, *10*, 8575−8578.
(29) Rostovtsev, V. V.; Green, L. G.; Fokin, V. V.; Sharpless, K. B. *Angew. Chem., Int. Ed.* **2002**, *41*, 2596−2599.
(30) Tornøe, C. W.; Christensen, C.; Meldal, M. *J. Org. Chem.* **2002**, *67*, 3057−3064.
(31) Gallagher-Duval, S.; Herve, G.; Sartori, G.; Enderlin, G.; Len, C. *New J. Chem.* **2013**, *37*, 1989−1995.
(32) McBride, L. J.; Kierzek, R.; Beaucage, S. L.; Caruthers, M. H. *J. Am. Chem. Soc.* **1986**, *108*, 2040−2048.
(33) Browne, D. L.; Harrity, J. P. A. *Tetrahedron* **2010**, *66*, 553−568.
(34) Barr, P. J.; Jones, A. S.; Serafinowski, P.; Walker, R. T. *J. Chem. Soc., Perkin Trans. 1* **1978**, 1263−1267.
(35) Baker, W.; Ollis, W. D. *Nature* **1946**, *158*, 703.
(36) Comas-Barceló, J.; Foster, R. S.; Fiser, B.; Gomez-Bengoa, E.; Harrity, J. P. A. *Chem. - Eur. J.* **2015**, *21*, 3257−3263.
(37) Kolodych, S.; Rasolofonjatovo, E.; Chaumontet, M.; Nevers, M.-C.; Créminon, C.; Taran, F. *Angew. Chem., Int. Ed.* **2013**, *52*, 12056−12060.
(38) Delaunay, T.; Es-Sayed, M.; Vors, J.-P.; Monteiro, N.; Balme, G. *Chem. Lett.* **2011**, *40*, 1434−1436.
(39) Knapp, D. M.; Gillis, E. P.; Burke, M. D. *J. Am. Chem. Soc.* **2009**, *131*, 6961−6963.
(40) Gryaznov, S. M.; Letsinger, R. L. *J. Am. Chem. Soc.* **1991**, *113*, 5876−5877.
(41) Hayakawa, Y.; Kawai, R.; Kataoka, M. *Eur. J. Pharm. Sci.* **2001**, *13*, 5−16.
(42) Ohkubo, A.; Seio, K.; Sekine, M. *Tetrahedron Lett.* **2004**, *45*, 363−366.
(43) Bishop, G. R.; Chaires, J. B. Characterization of DNA Structures by Circular Dichroism. *Current Protocols in Nucleic Acid Chemistry*; Wiley: New York, 2003; Unit 7.11, pp 7.11.1−7.11.8.
(44) Petersen, M.; Bondensgaard, K.; Wengel, J.; Jacobsen, J. P. *J. Am. Chem. Soc.* **2002**, *124*, 5974−5982.
(45) Gribble, G. W.; Hirth, B. H. *J. Heterocycl. Chem.* **1996**, *33*, 719−726.
(46) Qiu, D.; Shenkin, P. S.; Hollinger, F. P.; Still, W. C. *J. Phys. Chem. A* **1997**, *101*, 3005−3014.
(47) Pipek, J.; Mezey, P. G. *J. Chem. Phys.* **1989**, *90*, 4916−4926.

DOI: 10.1021/acs.joc.5b01577
J. Org. Chem. 2015, 80, 9592−9602